Environmental Science & Technology LETTERS

pubs.acs.org/journal/estlcu

Letter

Flame-Free Candles Are Not Pollution-Free: Scented Wax Melts as a Significant Source of Atmospheric Nanoparticles

Satya S. Patra, Jinglin Jiang, Jianghui Liu, Gerhard Steiner, Nusrat Jung,* and Brandon E. Boor*

Cite This: *Environ. Sci. Technol. Lett.* 2025, 12, 175−182

Read Online

ACCESS | Metrics & More | Article Recommendations | Supporting Information

ABSTRACT: Scented wax melts are being popularized as a safer, nontoxic alternative to traditional candles and incense for indoor aromatherapy. We performed field measurements in a residential test house to investigate atmospheric nanoparticle formation from scented wax melt use. We employed a high-resolution particle size magnifier-scanning mobility particle sizer (PSMPS) and a proton transfer reaction time-of-flight mass spectrometer (PTR-TOF-MS) for real-time monitoring of indoor atmospheric nanoparticle size distributions and terpene mixing ratios, respectively. Our findings reveal that terpenes released from scented wax melts react with indoor atmospheric ozone (O_3) to initiate new particle formation (NPF) events, resulting in significant indoor atmospheric nanoparticle concentrations ($>10^6$ cm^{-3}) comparable to those emitted by combustion-based scented candles, gas stoves, diesel engines, and natural gas engines. We show that scented wax melt-initiated NPF events can result in significant respiratory exposures, with nanoparticle respiratory tract deposited dose rates similar to those determined for combustion-based sources. Our results challenge the perception of scented wax melts as a safer alternative to combustion-based aromatherapy, highlighting the need for further research on the toxicological properties of the newly formed nanoparticles to better understand their environmental health implications.

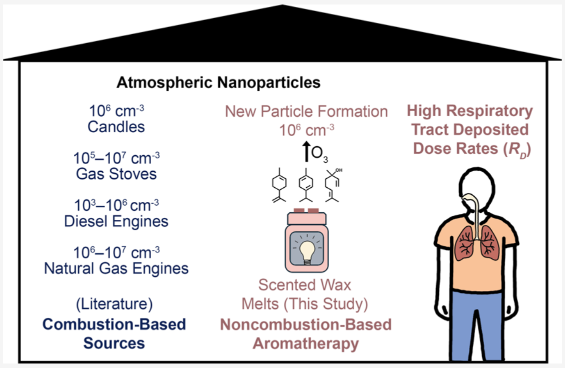

KEYWORDS: *nanoparticle pollution, new particle formation, indoor air quality, secondary organic aerosol, respiratory exposure*

INTRODUCTION

Scented wax melts have become a popular, stylish, and aromatic alternative to traditional candles and incense. These small pieces of scented wax release pleasant fragrances into homes, offices, and other indoor environments when heated without an open flame. Marketed as noncombustion, smoke-free, and nontoxic, scented wax melts are perceived as safer and cleaner options for indoor aromatherapy.[1] The scented wax melt market is rapidly expanding, as evidenced by its prominent presence in the product lines of numerous leading home fragrance companies.

Despite being flame-free and smoke-free, scented wax melts can emit quantities of volatile organic compounds (VOCs) that are larger than those of traditional scented candles[2] due to their higher fragrance concentration and the direct heating of wax, maximizing the melted wax surface area.[1] Manufacturers often highlight this advantage, claiming that scented wax melts quickly and efficiently fill indoor spaces with aroma. However, these VOCs, primarily composed of monoterpenes and their oxygenated derivatives, monoterpenoids, are highly reactive with atmospheric ozone (O_3), even at low O_3 concentrations.[3,4] Studies report that indoor sources emitting monoterpenes and monoterpenoids can react with indoor atmospheric O_3 to induce new particle formation (NPF; nucleation and subsequent growth of nanoparticles) in environments with low nitrogen monoxide (NO) concentrations.[3−11] Because scented wax melts do not involve combustion, they likely do not emit NO, suggesting possibilities for secondary reactions that could initiate NPF, despite being smoke-free. However, this phenomenon in indoor environments remains unexplored.

Here, we present the first comprehensive evaluation of nanoparticle formation using scented wax melts in a full-scale, mechanically ventilated residential test house. Utilizing advanced measurement techniques, including a high-resolution particle size magnifier-scanning mobility particle sizer (PSMPS)[12] and a proton transfer reaction time-of-flight mass spectrometer (PTR-TOF-MS),[13] we quantitatively demonstrate that secondary chemistry during scented wax melt use can form and grow indoor atmospheric nanoparticles, significantly enriching the sub-100 nm particle concentration in the indoor environment. Surprisingly, the indoor atmospheric nanoparticle concentrations from noncombustion-based

Received: November 19, 2024
Revised: December 28, 2024
Accepted: December 30, 2024
Published: February 3, 2025

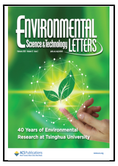

https://doi.org/10.1021/acs.estlett.4c00986

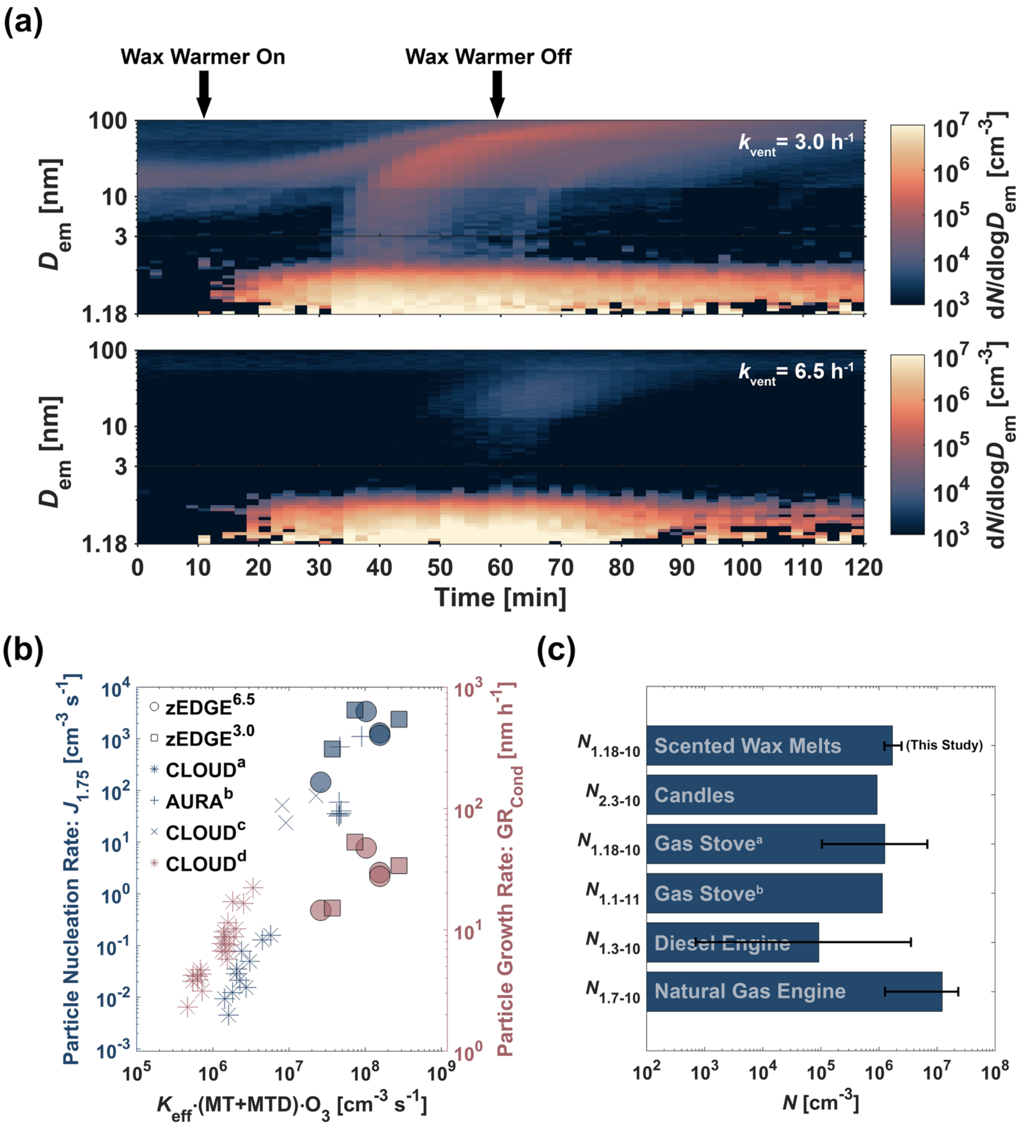

Figure 1. (a) Representative time-resolved evaluation of indoor atmospheric nucleation and growth (NPF) during the use of bergamot-scented wax melts (two cubes) in the Purdue zEDGE test house at two different outdoor air ventilation rates [k_{vent} values of 3.0 h^{-1} (top) and 6.5 h^{-1} (bottom)]. (b) Relationship between the effective terpene ozonolysis rates [K_{eff}·(MT + MTD)·O$_3$] and particle nucleation rates at the critical diameter ($J_{1.75}$) (left y-axis), along with mean condensational growth rates for particles in the size range of 3 nm < d_{em} < 10 nm (right y-axis) during NPF events initiated by scented wax melts. Legend: zEDGE$^{6.5}$, scented wax melts used in the zEDGE test house at a k_{vent} of 6.5 h^{-1}; zEDGE$^{3.0}$, scented wax melts used in the zEDGE test house at a k_{vent} of 3.0 h^{-1}; CLOUD^a, particle nucleation rates ($J_{1.7}$) from ref 24; AURA^b, particle nucleation rates ($J_{1.7}$) from ref 28; CLOUD^c, particle nucleation rates ($J_{1.7}$) from ref 29; CLOUD^d, apparent particle growth rates (3.2 nm < d_{em} < 8 nm) from ref 30. (c) Comparison of size-integrated sub-10 nm atmospheric nanoparticle number concentrations from scented wax melt use (this study) vs scented candle combustion (ref 31), gas stove combustion (Gas Stove^a, indoor bulk air measurements from ref 12; Gas Stove^b, cookstove emission hood measurements from ref 32), diesel engine (exhaust emission measurements at 75% engine load from ref 33), and natural gas engine (exhaust emission measurements, where the value represents the mean, calculated from the engine operating under both lower- and higher-torque conditions, from ref 34). The error bars for this study and for Gas Stove^a represent the 25th and 75th percentile values, whereas for the diesel engine, they represent the values at 50% and 100% engine loads. For the natural gas engine, the error bars correspond to the values under lower- and higher-torque operating conditions.

scented wax melts were similar to those emitted by combustion-based scented candles, gas stoves, diesel engines, and natural gas engines. Furthermore, the adult nanoparticle respiratory tract deposited dose rates while using scented wax melts rivaled those determined for combustion-based sources. Therefore, contrary to the perception of being a safer alternative, NPF events from noncombustion scented wax melts result in nanoparticle formation comparable to primary nanoparticle emissions from combustion-based sources.

■ METHODS AND MATERIALS

Field measurements of atmospheric nanoparticle formation and growth during the use of scented wax melts for room fragrance were performed in the Purdue zero Energy Design Guidance for Engineers (zEDGE) test house. A detailed description of the test house can be found elsewhere.[2,12−17] The activity sequence for the use of wax melts in the test house is summarized in the Supporting Information.

Real-time measurements of atmospheric nanoparticle number concentrations and size distributions from 1.18 to

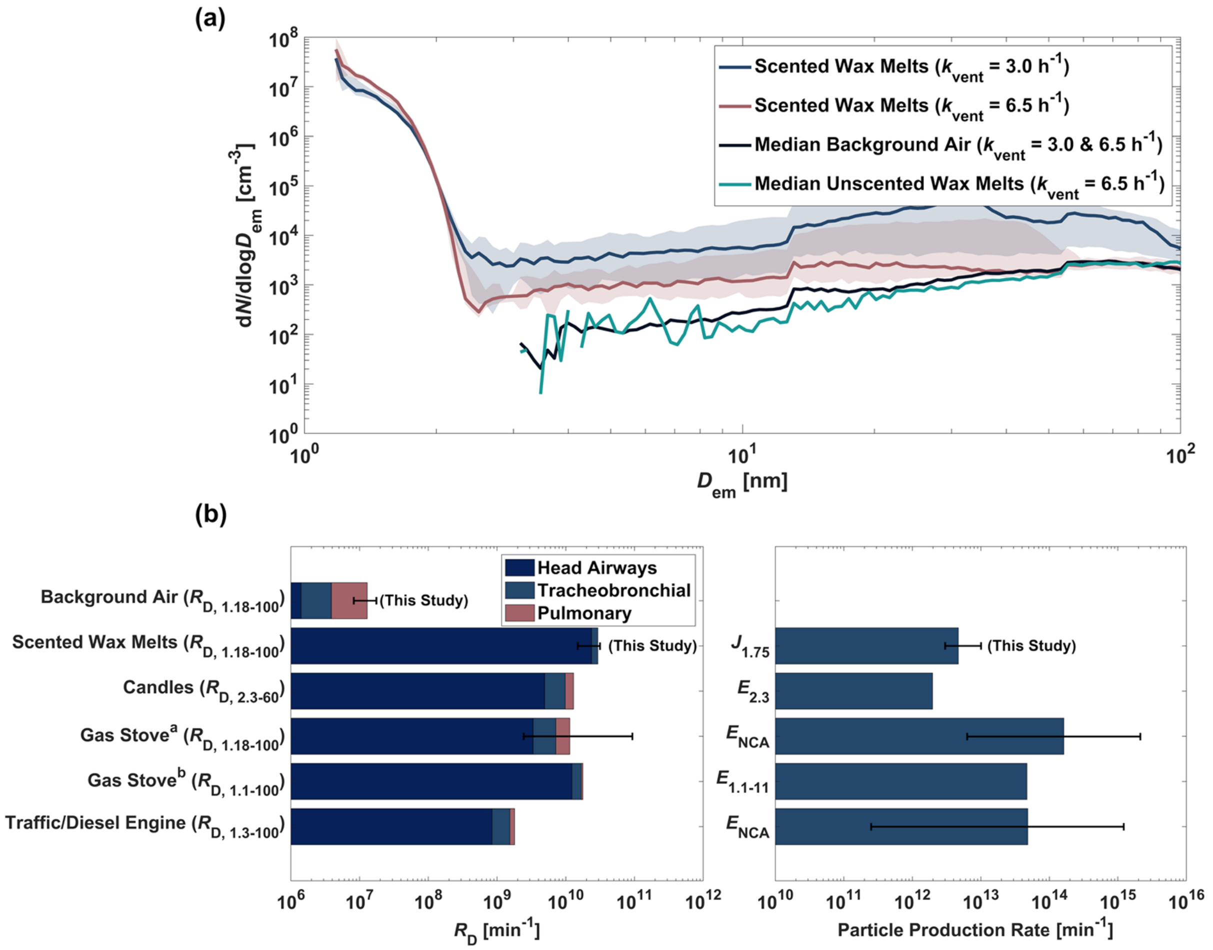

Figure 2. (a) Comparison of median particle number size distributions during NPF events initiated by three different scented wax melts used at two different outdoor air ventilation rates (k_{vent} values of 3.0 and 6.5 h^{-1}) in the Purdue zEDGE test house. The shaded area presents the 25th and 75th percentiles of the particle number size distributions. The plot also includes the median particle number size distribution of background air in the Purdue zEDGE test house without activity, as well as the median particle number size distribution during the use of unscented wax melts in the Purdue zEDGE test house. (b) Comparison of (left) median respiratory tract deposited dose rates (R_D) of 1.18−100 nm particles in various respiratory tract regions (head airways, tracheobronchial, and pulmonary) of adults during NPF events initiated by scented wax melt use (this study) vs R_D during scented candle combustion (ref 31), gas stove combustion (Gas Stove^a, indoor bulk air measurements from ref 12; Gas Stove^b, cookstove emission hood measurements from ref 32), and measurements near a roadside environment from ref 33. The *y*-axis label specifies the size range for the R_D calculation. The plot also includes the median R_D of background air in the Purdue zEDGE test house without activity. Comparison of (right) particle production rates for scented wax melt use at 1.75 nm (this study) vs the particle production rates during indoor scented candle combustion (ref 31), gas stove combustion (Gas Stove^a, indoor bulk air measurements from ref 12; Gas Stove^b, cookstove emission hood measurements from ref 32), and diesel engine (exhaust emission measurements at 75% engine load from ref 33). The *y*-axis label specifies the size range for which the particle production rates were calculated. The particle production rates for scented wax melt use are calculated as the product of the mean particle nucleation rates during NPF events and the volume of the Purdue zEDGE test house. The method for estimating particle production rates in min^{-1} from particle emission factors in $kg\text{-}fuel^{-1}$ for refs 32 and 33 is detailed in the Supporting Information. The error bars for this study and for Gas Stove^a represent the 25th and 75th percentile values, whereas for the diesel engine, they represent the values at 50% and 100% engine loads. Note that both the background particle number size distributions and the particle number size distributions during the use of scented and unscented wax melts were subjected to background charger ion correction in the sub-3 nm size range (as detailed in the Supporting Information).

572.5 nm were conducted using two different aerosol instruments: a novel PSMPS (GRIMM Aerosol Technik Ainring GmbH & Co. KG, Ainring, Germany) and a scanning mobility particle sizer (SMPS) equipped with a long differential mobility analyzer (DMA) (model 3938NL88, TSI Inc., Shoreview, MN).[12,18] The PSMPS detects and classifies atmospheric nanoparticles down to ∼1 nm.[19] VOC mixing ratios were measured using a PTR-TOF-MS (model PTR-TOF 4000, Ionicon Analytik GmbH, Innsbruck, Austria). Other trace gas instrumentation used in the measurement campaign included NO_x ($NO + NO_2$), carbon dioxide (CO_2), and O_3 analyzers. Additional details about the instrument configuration, setup, and data analysis are discussed in the Supporting Information.

To evaluate nanoparticle dynamics during scented wax melt use, we estimated the particle nucleation rate at the critical diameter ($J_{1.75}$, in cm^{-3} s^{-1}) using the discrete aerosol general dynamics equation (GDE) in a Eulerian specification (eq 1).[12,20]

$$J_{1.75} = \left(\frac{\mathrm{d}N_{1.75-u}}{\mathrm{d}t} + \sum_{d_\mathrm{p}=1.75}^{u} k_{\mathrm{vent}} \times N_{d_{\mathrm{p},i}} + \sum_{d_\mathrm{p}=1.75}^{u} k_{\mathrm{dep},d_\mathrm{p}} \times N_{d_{\mathrm{p},i}} + \sum_{d_\mathrm{p}=1.75}^{u} \mathrm{CoagSnk}_{d_\mathrm{p}} \times N_{d_{\mathrm{p},i}} - \sum_{d_\mathrm{p}=1.75}^{u} \mathrm{CoagSrc}_{d_\mathrm{p}} + C_u \times N_{u,i} \right) \quad (1)$$

The terms in eq 1 are explained in detail in the Supporting Information. For the scented wax melts that exhibited particle nucleation and growth beyond 3 nm, a composition-weighted effective terpene ozonolysis rate constant (K_{eff}, in $\mathrm{cm}^3\ \mathrm{s}^{-1}$) was determined using the terpene isomer compositions and their respective second-order ozonolysis rate constants (as detailed in the Supporting Information). Furthermore, following methods from previous studies,[12,16,21] we estimated respiratory tract deposited dose rates (R_D, in min^{-1}) to assess the rate of deposition of nanoparticles formed during the use of scented wax melts in various respiratory tract regions (head airways, tracheobronchial, and pulmonary) of adults.

RESULTS AND DISCUSSION

New Particle Formation during Scented Wax Melt Use. The use of scented wax melts in the test house led to significant emissions of terpenes [monoterpenes and monoterpenoids (MT + MTD)] to indoor air (Table S1). This occurred when the mean background indoor atmospheric O_3 and NO mixing ratios were 9.7–29.9 and 0.6–0.8 ppb, respectively. Terpenes released during scented wax melt use consume indoor atmospheric O_3 to form peroxy and hydroperoxy radicals ($RO_2^\bullet$ and $HO_2^\bullet$). $RO_2^\bullet$ can react with NO, $HO_2^\bullet$, and other peroxy radicals. Although a reduction in O_3 is expected to increase indoor atmospheric NO concentrations, $RO_2^\bullet$ and $HO_2^\bullet$ rapidly react with NO, likely offsetting the expected increase and thereby stabilizing NO mixing ratios during scented wax melt use.[4] The NO concentrations in the test house were sufficiently low (≤0.8 ppb) that O_3-initiated autoxidation of terpenes can compete with other $RO_2^\bullet$ reactions.[5,22] This process is known to produce various highly oxygenated molecules, a subset of which can drive the pure biogenic nucleation of atmospheric particles.[23−25]

Particle nucleation was observed during all scented wax melt activities (Figures S2 and S3), increasing the number concentrations of indoor atmospheric nanocluster aerosol (NCA, sub-3 nm particles). However, freshly nucleated particles grew past the sub-3 nm size range (Figure 1a and Figure S3) for only those scented wax melts that emitted higher mixing ratios of terpenes (median peak MT + MTD = 193.4 ppb for particle nucleation and growth events; median peak MT + MTD = 55 ppb for particle nucleation but no growth events). This size range is particularly significant because sub-3 nm particles are prone to coagulation and evaporation loss and require more low-volatility condensational vapors to offset this loss.[26] Thus, particle growth beyond the sub-3 nm size range was observed for only scented wax melts with higher terpene emissions, and this growth occurred as the terpene emissions approached their peak (Figure 1 and Figure S6). Another reason not all freshly nucleated particles grew past the sub-3 nm size range during scented wax melt use could be the greater abundance of less O_3-reactive terpene VOCs, such as menthol and menthone. In contrast, wax melts that showed particle nucleation and growth past the sub-3 nm size range might contain more O_3-reactive terpene VOCs, such as d-limonene and linalool. These are effective in forming larger quantities of low-volatility condensational vapors that drive particle growth.[3,27] Future studies are needed to measure low-volatility condensable vapors using various high-resolution chemical ionization mass spectrometers during the use of scented wax melts to fully understand nanoparticle growth dynamics.

In scenarios in which particle nucleation and growth past 3 nm were observed, the particle nucleation and condensational growth rates followed the trend of the effective terpene ozonolysis rates [$K_{\mathrm{eff}}\cdot(\mathrm{MT} + \mathrm{MTD})\cdot O_3$] (Figure 1b). This observation suggests that the precursor terpene emissions and their ozonolysis are responsible for the particle nucleation and growth observed during the use of scented wax melts. To further confirm this, we tested an unscented wax melt in the wax warmer in the test house. No significant terpene emissions or particle nucleation and growth occurred during its use (Table S1 and Figure S4), reinforcing the idea that the precursor terpene emissions from scented wax melts are responsible for NPF when using scented wax melts. Additionally, the particle number size distributions during unscented wax melt use showed no major deviation when compared with the background particle number size distributions in the test house, suggesting that the vapors produced from melting unscented wax do not contribute to particle growth (Figure 2a). Terpene emissions dominated the VOC emissions during scented wax melt use. Other than terpenes, we observed a minor increase in sesquiterpene (SQT) mixing ratios during the use of scented wax melts (Figure S5 and Table S3; the mixing ratios might be underestimated due to fragmentation of the protonated SQT). However, compared with the peak MT + MTD emissions, the average ratio of the increased peak SQT mixing ratios to the peak MT + MTD mixing ratios is ∼0.16% (Table S3), which is significantly lower than the SQT to MT ratio found in chamber experiments known to influence biogenic new particle formation (2%).[35] Therefore, the very high MT + MTD emissions from scented wax melts should primarily drive the production of nanoparticles during their use. Nevertheless, the role of SQT in this process cannot be entirely dismissed and warrants future controlled studies to clarify the contribution of SQT to biogenic new particle formation at such low SQT to MT ratios.

Figure 1a illustrates typical indoor atmospheric NPF events during the use of scented wax melts at two different outdoor air ventilation rates (k_{vent} values of 3.0 and 6.5 h^{-1}). Particle nucleation commenced a few minutes after the wax warmer was switched on, with size-integrated (1.18–3 nm) NCA number concentrations (N_{NCA}) increasing sharply from background concentrations of $\sim 10^2$ to $>10^4\ \mathrm{cm}^{-3}$. N_{NCA} remained elevated throughout the operation of the wax warmer. Interestingly, NCA concentrations remained high even after the wax warmer was turned off (Figure 1a and Figures S2 and S3) due to sustained nucleation driven by elevated terpene mixing ratios (Figure S6). The particle growth plume out of the NCA size fraction emerged later, coinciding with increasing terpene emissions nearing their peak.

A key observation is that while the particles in the NCA size fraction appeared similar at both outdoor air ventilation rates, the growth plume was markedly stronger at the lower ventilation rate (Figure 1a). We further examined this by comparing the median particle number size distributions during the use of three different scented wax melts under two ventilation rates (Figure 2a). The particle number size distributions revealed that in the NCA size fraction, particularly for particles smaller than 2 nm, there was minimal difference in the particle number concentrations between the two ventilation rates. Median N_{NCA} values during this period were 1.4×10^6 cm^{-3} at a k_{vent} of 3.0 h^{-1} and 2.3×10^6 cm^{-3} at a k_{vent} of 6.5 h^{-1}. However, significantly more particles in the 3−100 nm size range were present at the lower ventilation rate (median N_{3-100} values of 4.9×10^4 cm^{-3} at a k_{vent} of 3.0 h^{-1} and 2.7×10^3 cm^{-3} at a k_{vent} of 6.5 h^{-1}). To further investigate the potential reasons for this observed phenomenon, we estimated the survival probabilities of indoor atmospheric nanoparticles from 1.75 to 10 nm ($P_{1.75\rightarrow10}$; estimation methods discussed in the Supporting Information) during scented wax melt use activities that exhibited particle nucleation and growth beyond 3 nm (Table S5). Nanoparticle survival is typically linked to either the presence of low-volatility condensable gases or the background sink.[36] In the zEDGE test house, the background sink levels before the use of scented wax melts were relatively similar (Table S1), suggesting that low-volatility condensable gases likely governed nanoparticle survival. Although we did not measure low-volatility species in this study, the effective terpene ozonolysis rates [$K_{\mathrm{eff}}\cdot(\mathrm{MT} + \mathrm{MTD})\cdot\mathrm{O_3}$] and the condensational growth rates ($\mathrm{GR_{Cond}}$) are reported to be proportional to the presence of these gases.[30] We observed that both these rates were higher at an outdoor air ventilation rate of 3.0 h^{-1} than at a k_{vent} of 6.5 h^{-1} (Figure 1b), likely due to higher terpene mixing ratios at the lower k_{vent} (Table S1). Consequently, $P_{1.75\rightarrow10}$ was observed to be higher at the lower k_{vent} (Table S5), which presumably explains why both the particle growth plume and the concentrations of 3−100 nm particles were higher at lower outdoor air ventilation rates during the use of scented wax melts. For NCA, while the particle nucleation rate increased at lower k_{vent} values (Figure 1b), previous studies suggest that at lower k_{vent} values, NCA coagulation loss rates also increase.[37] Thus, the higher loss rates might offset the increased particle nucleation rates at lower outdoor air ventilation rates, causing the NCA concentrations to remain relatively consistent across different ventilation rates during the use of scented wax melts. These novel observations highlight the impact of outdoor air ventilation on the indoor NPF dynamics.

Quantifying NPF during Scented Wax Melt Use and Comparisons with Combustion Sources. To quantify the rate of formation of new particles while considering indoor-specific loss processes, we estimated particle nucleation rates ($J_{1.75}$) for NPF events initiated during scented wax melt use (eq 1). Our observations revealed remarkably high values of $J_{1.75}$ during these NPF events, with mean $J_{1.75}$ values ranging from 143 to 3588 cm^{-3} s^{-1}. This variability can be attributed to the differing effective terpene ozonolysis rates [$K_{\mathrm{eff}}\cdot(\mathrm{MT} + \mathrm{MTD})\cdot\mathrm{O_3}$] for different scented wax melts (Figure 1b). Notably, the particle nucleation rates during the use of scented wax melts indoors are orders of magnitude higher than typical outdoor atmospheric particle nucleation rates (~0.1 to 100 cm^{-3} s^{-1}),[26,38,39] characterizing these NPF events as intense. Furthermore, the nucleation rates observed here correlate strongly with the previously published $J_{1.7}$ values and terpene ozonolysis reaction rates from studies conducted in CLOUD[24,29] and AURA[28] chambers on terpene-induced particle nucleation. This agreement further corroborates that terpene ozonolysis is the likely mechanism for nucleation initiated by the use of scented wax melts, with the significant terpene emissions from these products explaining the high nucleation rates observed. As reported for NPF in both indoor and outdoor environments,[11,20] coagulation loss contributes the most to the estimated $J_{1.75}$ (~58%) (Figure S7). The second largest contributor to $J_{1.75}$ is the coagulation source [~33% (Figure S7)], which is often overlooked in indoor nanoparticle dynamics models.

Expressed as particles per minute, the mean net particle production rate at 1.75 nm during these NPF events in the test house was 6.4×10^{12} min^{-1}, ~3 times higher than the reported particle emission rate at 2.3 nm during indoor candle combustion [1.9×10^{12} min^{-1} (Figure 2b)].[31] While Wallace et al.[31] reported emission rates at a lower limit of 2.3 nm, precluding a direct comparison at 1.75 nm, Torkmahalleh et al.[40] reported a mean 1−3 nm particle concentration of 1.1×10^6 cm^{-3} during a day with two candle-burning events in a school. In our study, the mean size-integrated (1.18−3 nm) NCA number concentration during NPF events initiated by scented wax melts was 1.9×10^6 cm^{-3}, indicating that the particle concentrations from scented wax melt use can be as high as those from candle burning. Upon comparison of scented wax melt-initiated NPF events with other indoor secondary NCA sources, scented wax melt-initiated NPF events can generate more indoor atmospheric NCA than monoterpene ozonolysis during indoor mopping[4] ($N_{\mathrm{NCA}} \sim 10^5$ cm^{-3}) or indoor 3D printing[41] ($N_{\mathrm{NCA}} \sim 10^2$–$10^5$ cm^{-3}). Furthermore, compared to other combustion sources, NCA concentrations formed during scented wax melt-initiated NPF events can reach levels similar to those emitted during the operation of indoor cookstoves ($N_{\mathrm{NCA}} \sim 10^5$–$10^7$ cm^{-3}),[12,32] as well as exhaust emissions from diesel engines ($N_{\mathrm{NCA}} \sim 10^3$–$10^6$ cm^{-3})[33] and natural gas engines ($N_{\mathrm{NCA}} \sim 10^6$–$10^7$ cm^{-3}).[34] Additionally, particle production rates observed during NPF events initiated by scented wax melts can attain magnitudes comparable to those reported during the operation of indoor cookstoves and diesel engines (Figure 2b). Therefore, despite being combustion-free, using scented wax melts can be a significant source of indoor atmospheric NCA.

The high terpene emissions during scented wax melt use, which initiated the NPF events, drove very high particle condensational growth rates ($\mathrm{GR_{Cond}}$) of NCA to greater than 3 nm, reaching ~100 nm during strong NPF events (Figure 1a and Figure S3). The mean $\mathrm{GR_{Cond}}$ from 3 to 10 nm during the use of scented wax melts ranged from 14.5 to 52.8 nm h^{-1} (Figure 1b), significantly higher than the growth rates observed for outdoor atmospheric NPF events, which are approximately 1−10 nm h^{-1}.[26] As a result, the NPF events initiated by scented wax melt use not only increased indoor atmospheric NCA concentrations but also increased the particle number concentrations for particles greater than 3 nm (Figures 1a and 2a). Therefore, our observations of sub-3 nm particles and particles greater than 3 nm during noncombustion-based scented wax melt use in the test house suggest that the use of scented wax melts indoors drives intense indoor atmospheric particle nucleation and growth, even at low indoor $\mathrm{O_3}$ mixing ratios (<10 ppb). This results in extremely high indoor atmospheric nanoparticle concentrations.

Atmospheric Implications of Scented Wax Melt Use. Significant particle formation during the use of scented wax melts can pose a major respiratory inhalation burden on indoor occupants. In our study, during NPF events triggered by scented wax melt use in the test house, the respiratory tract deposited dose rates (R_D) for 1.18−100 nm particles ranged from 1.4×10^{10} to 3.3×10^{10} min^{-1}, with a median R_D of 2.9×10^{10} min^{-1}. For comparison, the background R_D in the test house ranged from 8×10^6 to 1.9×10^7 min^{-1}, with a median R_D of 1.3×10^7 min^{-1}, which is 3 orders of magnitude smaller than the R_D during the use of scented wax melts. A majority of the scented wax melt-formed particles are deposited in the upper respiratory tract regions (Figure 2b). Because of their small size, once deposited, these particles can migrate between cells, enter the bloodstream, and possibly reach organs like the liver and brain.[42,43] Furthermore, the R_D for 1.18−100 nm particles in the pulmonary region can reach 2×10^8 min^{-1} during the use of scented wax melts. This is alarming, as these nanoparticles, formed in occupied environments, can also reach very high doses in the deeper regions of the lungs. What is more concerning is that the respiratory tract deposited dose rates are comparable to those observed for indoor scented candle combustion, indoor gas stove combustion, and near a roadside environment, with R_D values of 1.3×10^{10}, 1.2×10^{10}, and 1.8×10^9 min^{-1}, respectively (Figure 2b). Therefore, counterintuitively, although they are marketed as a safer alternative, the particle number-based inhalation exposure associated with noncombustion-based scented wax melts is similar to those posed by combustion-based scented products like candles and gas stoves.

Recent studies underscore the health risks associated with inhaling nanoparticles formed through the ozonolysis of terpenes (the mechanism responsible for nanoparticle formation when using scented wax melts; discussed in detail in the Supporting Information).[44−46] Moreover, Pye et al.[47] report that terpene nanoparticles are associated with approximately five additional cardiorespiratory deaths per 100 000 people in the United States. Therefore, considering the high respiratory tract deposited dose rates from using scented wax melts and evidence suggesting that these particles can have detrimental effects on respiratory health, careful consideration of their use is recommended despite the scented wax melts being marketed as a safer alternative for indoor aromatherapy. Future studies are needed to better understand the speciation of VOCs emitted by scented wax melts by using gas chromatography measurements and to conduct toxicological evaluations of the nanoparticles formed during their use.

■ ASSOCIATED CONTENT

Supporting Information

The Supporting Information is available free of charge at https://pubs.acs.org/doi/10.1021/acs.estlett.4c00986.

> Details of the experimental protocol, nanoparticle and gas-phase measurement equipment, indoor atmospheric nanoparticle dynamics modeling, effective terpene ozonolysis rate constant calculation, nanoparticle survival probability estimation, and health effects of terpene nanoparticles; summary of the wax melts used; and time-resolved evaluation of nanoparticle size distributions during their use in the Purdue zEDGE test house (PDF)

■ AUTHOR INFORMATION

Corresponding Authors

Nusrat Jung − *Lyles School of Civil and Construction Engineering, Purdue University, West Lafayette, Indiana 47907, United States; Ray W. Herrick Laboratories, Center for High Performance Buildings, Purdue University, West Lafayette, Indiana 47907, United States;* orcid.org/0000-0002-8874-8923; Email: nusratj@purdue.edu

Brandon E. Boor − *Lyles School of Civil and Construction Engineering, Purdue University, West Lafayette, Indiana 47907, United States; Ray W. Herrick Laboratories, Center for High Performance Buildings, Purdue University, West Lafayette, Indiana 47907, United States;* orcid.org/0000-0003-1011-4100; Email: bboor@purdue.edu

Authors

Satya S. Patra − *Lyles School of Civil and Construction Engineering, Purdue University, West Lafayette, Indiana 47907, United States; Ray W. Herrick Laboratories, Center for High Performance Buildings, Purdue University, West Lafayette, Indiana 47907, United States;* orcid.org/0000-0003-2099-7875

Jinglin Jiang − *Lyles School of Civil and Construction Engineering, Purdue University, West Lafayette, Indiana 47907, United States; Ray W. Herrick Laboratories, Center for High Performance Buildings, Purdue University, West Lafayette, Indiana 47907, United States; School of Architectural Engineering, Changzhou Vocational Institute of Engineering, Changzhou, Jiangsu 213164, China;* orcid.org/0000-0001-6271-0436

Jianghui Liu − *Lyles School of Civil and Construction Engineering, Purdue University, West Lafayette, Indiana 47907, United States*

Gerhard Steiner − *GRIMM Aerosol Technik Ainring GmbH & Co. KG, Ainring 83404, Germany*

Complete contact information is available at:
https://pubs.acs.org/10.1021/acs.estlett.4c00986

Notes

The authors declare the following competing financial interest(s): G.S. is a full-time employee of GRIMM Aerosol Technik Ainring GmbH & Co. KG, which has a potential direct or indirect financial interest in the subject matter discussed in this work.

■ ACKNOWLEDGMENTS

Financial support was provided by the National Science Foundation (CBET-1847493 to B.E.B.), Purdue University start-up funds (to N.J.), and an American Society of Heating, Refrigerating, and Air Conditioning Engineers Graduate Student Grant-In-Aid Award (to S.S.P.).

■ REFERENCES

(1) Cassidy, G. 12 Great Reasons to Use Wax Melts vs Candles. https://www.purcellandwoodcock.com/blog/wax-melts-vs-candles.html (accessed 2024-06-24).

(2) Liu, J.; Jiang, J.; Ding, X.; Patra, S. S.; Cross, J. N.; Huang, C.; Kumar, V.; Price, P.; Reidy, E. K.; Tasoglou, A.; Huber, H.; Stevens, P. S.; Boor, B. E.; Jung, N. Real-Time Evaluation of Terpene Emissions and Exposures during the Use of Scented Wax Products in Residential Buildings with PTR-TOF-MS. *Build. Environ.* **2024**, *255*, 111314.

(3) Fu, Z.; Guo, S.; Yu, Y.; Xie, H.-B.; Li, S.; Lv, D.; Zhou, P.; Song, K.; Chen, Z.; Tan, R.; Hu, K.; Shen, R.; Yao, M.; Hu, M. Oxidation Mechanism and Toxicity Evolution of Linalool, a Typical Indoor Volatile Chemical Product. *Environ. Health* **2024**, *2* (7), 486−498.

(4) Rosales, C. M. F.; Jiang, J.; Lahib, A.; Bottorff, B. P.; Reidy, E. K.; Kumar, V.; Tasoglou, A.; Huber, H.; Dusanter, S.; Tomas, A.; Boor, B. E.; Stevens, P. S. Chemistry and Human Exposure Implications of Secondary Organic Aerosol Production from Indoor Terpene Ozonolysis. *Sci. Adv.* **2022**, *8* (8), No. eabj9156.

(5) Pagonis, D.; Algrim, L. B.; Price, D. J.; Day, D. A.; Handschy, A. V.; Stark, H.; Miller, S. L.; de Gouw, J. A.; Jimenez, J. L.; Ziemann, P. J. Autoxidation of Limonene Emitted in a University Art Museum. *Environ. Sci. Technol. Lett.* **2019**, *6* (9), 520−524.

(6) Vartiainen, E.; Kulmala, M.; Ruuskanen, T. M.; Taipale, R.; Rinne, J.; Vehkamäki, H. Formation and Growth of Indoor Air Aerosol Particles as a Result of D-Limonene Oxidation. *Atmos. Environ.* **2006**, *40* (40), 7882−7892.

(7) Youssefi, S.; Waring, M. S. Transient Secondary Organic Aerosol Formation from Limonene Ozonolysis in Indoor Environments: Impacts of Air Exchange Rates and Initial Concentration Ratios. *Environ. Sci. Technol.* **2014**, *48* (14), 7899−7908.

(8) Waring, M. S.; Wells, J. R.; Siegel, J. A. Secondary Organic Aerosol Formation from Ozone Reactions with Single Terpenoids and Terpenoid Mixtures. *Atmos. Environ.* **2011**, *45* (25), 4235−4242.

(9) Waring, M. S. Secondary Organic Aerosol Formation by Limonene Ozonolysis: Parameterizing Multi-Generational Chemistry in Ozone- and Residence Time-Limited Indoor Environments. *Atmos. Environ.* **2016**, *144*, 79−86.

(10) Singer, B. C.; Coleman, B. K.; Destaillats, H.; Hodgson, A. T.; Lunden, M. M.; Weschler, C. J.; Nazaroff, W. W. Indoor Secondary Pollutants from Cleaning Product and Air Freshener Use in the Presence of Ozone. *Atmos. Environ.* **2006**, *40* (35), 6696−6710.

(11) Patra, S. S.; Liu, J.; Jiang, J.; Ding, X.; Huang, C.; Keech, C.; Steiner, G.; Stevens, P. S.; Jung, N.; Boor, B. E. Rapid Nucleation and Growth of Indoor Atmospheric Nanocluster Aerosol during the Use of Scented Volatile Chemical Products in Residential Buildings. *ACS ES&T Air* **2024**, *1* (10), 1276−1293.

(12) Patra, S. S.; Jiang, J.; Ding, X.; Huang, C.; Reidy, E. K.; Kumar, V.; Price, P.; Keech, C.; Steiner, G.; Stevens, P.; Jung, N.; Boor, B. E. Dynamics of Nanocluster Aerosol in the Indoor Atmosphere during Gas Cooking. *PNAS Nexus* **2024**, *3* (2), pgae044.

(13) Jiang, J.; Ding, X.; Patra, S. S.; Cross, J. N.; Huang, C.; Kumar, V.; Price, P.; Reidy, E. K.; Tasoglou, A.; Huber, H.; Stevens, P. S.; Boor, B. E.; Jung, N. Siloxane Emissions and Exposures during the Use of Hair Care Products in Buildings. *Environ. Sci. Technol.* **2023**, *57* (48), 19999−20009.

(14) Ding, X.; Lu, H.; Jiang, J.; Tasoglou, A.; Shah, A. D.; Jung, N. Real-Time Indoor Sensing of Volatile Organic Compounds during Building Disinfection Events via Photoionization Detection and Proton Transfer Reaction Mass Spectrometry. *Build. Environ.* **2023**, *246*, 110953.

(15) Ding, X.; Jiang, J.; Tasoglou, A.; Huber, H.; Shah, A. D.; Jung, N. Evaluation of Workplace Exposures to Volatile Chemicals During COVID-19 Building Disinfection Activities with Proton Transfer Reaction Mass Spectrometry. *Ann. Work Expo. Health* **2023**, *67* (4), 546−551.

(16) Jiang, J.; Ding, X.; Tasoglou, A.; Huber, H.; Shah, A. D.; Jung, N.; Boor, B. E. Real-Time Measurements of Botanical Disinfectant Emissions, Transformations, and Multiphase Inhalation Exposures in Buildings. *Environ. Sci. Technol. Lett.* **2021**, *8* (7), 558−566.

(17) Jiang, J.; Ding, X.; Isaacson, K. P.; Tasoglou, A.; Huber, H.; Shah, A. D.; Jung, N.; Boor, B. E. Ethanol-Based Disinfectant Sprays Drive Rapid Changes in the Chemical Composition of Indoor Air in Residential Buildings. *J. Hazard. Mater. Lett.* **2021**, *2*, 100042.

(18) Patra, S. S.; Ramsisaria, R.; Du, R.; Wu, T.; Boor, B. E. A Machine Learning Field Calibration Method for Improving the Performance of Low-Cost Particle Sensors. *Build. Environ.* **2021**, *190*, 107457.

(19) Steiner, G.; Flentje, H.; Väkevä, M.; Keck, L.; Vanhanen, J. Monitoring Ambient Aerosol Size Distributions from 1−55 nm with the GRIMM-AIRMODUS PSMPS. In *EGU General Assembly Conference Abstracts*; 2021; EGU21-12472.

(20) Cai, R.; Jiang, J. A New Balance Formula to Estimate New Particle Formation Rate: Reevaluating Effect of Coagulation Scavenging. *Atmos. Chem. Phys.* **2017**, *17* (20), 12659−12675.

(21) Wu, T.; Täubel, M.; Holopainen, R.; Viitanen, A.-K.; Vainiotalo, S.; Tuomi, T.; Keskinen, J.; Hyvärinen, A.; Hämeri, K.; Saari, S. E.; Boor, B. E. Infant and Adult Inhalation Exposure to Resuspended Biological Particulate Matter. *Environ. Sci. Technol.* **2018**, *52* (1), 237−247.

(22) Jokinen, T.; Sipilä, M.; Richters, S.; Kerminen, V.-M.; Paasonen, P.; Stratmann, F.; Worsnop, D.; Kulmala, M.; Ehn, M.; Herrmann, H.; Berndt, T. Rapid Autoxidation Forms Highly Oxidized RO_2 Radicals in the Atmosphere. *Angew. Chem. Int. Ed.* **2014**, *53* (52), 14596−14600.

(23) Kirkby, J.; Duplissy, J.; Sengupta, K.; Frege, C.; Gordon, H.; Williamson, C.; Heinritzi, M.; Simon, M.; Yan, C.; Almeida, J.; Tröstl, J.; Nieminen, T.; Ortega, I. K.; Wagner, R.; Adamov, A.; Amorim, A.; Bernhammer, A.-K.; Bianchi, F.; Breitenlechner, M.; Brilke, S.; et al. Ion-Induced Nucleation of Pure Biogenic Particles. *Nature* **2016**, *533* (7604), 521−526.

(24) Simon, M.; Dada, L.; Heinritzi, M.; Scholz, W.; Stolzenburg, D.; Fischer, L.; Wagner, A. C.; Kürten, A.; Rörup, B.; He, X.-C.; Almeida, J.; Baalbaki, R.; Baccarini, A.; Bauer, P. S.; Beck, L.; Bergen, A.; Bianchi, F.; Bräkling, S.; Brilke, S.; Caudillo, L.; et al. Molecular Understanding of New-Particle Formation from α-Pinene between −50 and + 25 °C. *Atmos. Chem. Phys.* **2020**, *20* (15), 9183−9207.

(25) Kirkby, J.; Amorim, A.; Baltensperger, U.; Carslaw, K. S.; Christoudias, T.; Curtius, J.; Donahue, N. M.; Haddad, I. El; Flagan, R. C.; Gordon, H.; Hansel, A.; Harder, H.; Junninen, H.; Kulmala, M.; Kürten, A.; Laaksonen, A.; Lehtipalo, K.; Lelieveld, J.; Möhler, O.; Riipinen, I.; et al. Atmospheric New Particle Formation from the CERN CLOUD Experiment. *Nat. Geosci.* **2023**, *16* (11), 948−957.

(26) Stolzenburg, D.; Cai, R.; Blichner, S. M.; Kontkanen, J.; Zhou, P.; Makkonen, R.; Kerminen, V.-M.; Kulmala, M.; Riipinen, I.; Kangasluoma, J. Atmospheric Nanoparticle Growth. *Rev. Mod. Phys.* **2023**, *95* (4), 45002.

(27) Khamaganov, V. G.; Hites, R. A. Rate Constants for the Gas-Phase Reactions of Ozone with Isoprene, α- and β-Pinene, and Limonene as a Function of Temperature. *J. Phys. Chem. A* **2001**, *105* (5), 815−822.

(28) Thomsen, D.; Iversen, E. M.; Skønager, J. T.; Luo, Y.; Li, L.; Roldin, P.; Priestley, M.; Pedersen, H. B.; Hallquist, M.; Ehn, M.; Bilde, M.; Glasius, M. The Effect of Temperature and Relative Humidity on Secondary Organic Aerosol Formation from Ozonolysis of Δ^3-Carene. *Environ. Sci.: Atmos.* **2024**, *4* (1), 88−103.

(29) Caudillo, L.; Rörup, B.; Heinritzi, M.; Marie, G.; Simon, M.; Wagner, A. C.; Müller, T.; Granzin, M.; Amorim, A.; Ataei, F.; Baalbaki, R.; Bertozzi, B.; Brasseur, Z.; Chiu, R.; Chu, B.; Dada, L.; Duplissy, J.; Finkenzeller, H.; Gonzalez Carracedo, L.; He, X.-C.; et al. Chemical Composition of Nanoparticles from α-Pinene Nucleation and the Influence of Isoprene and Relative Humidity at Low Temperature. *Atmos. Chem. Phys.* **2021**, *21* (22), 17099−17114.

(30) Stolzenburg, D.; Fischer, L.; Vogel, A. L.; Heinritzi, M.; Schervish, M.; Simon, M.; Wagner, A. C.; Dada, L.; Ahonen, L. R.; Amorim, A.; Baccarini, A.; Bauer, P. S.; Baumgartner, B.; Bergen, A.; Bianchi, F.; Breitenlechner, M.; Brilke, S.; Buenrostro Mazon, S.; Chen, D.; Dias, A.; et al. Rapid Growth of Organic Aerosol Nanoparticles over a Wide Tropospheric Temperature Range. *Proc. Natl. Acad. Sci. U. S. A.* **2018**, *115* (37), 9122−9127.

(31) Wallace, L.; Jeong, S.-G.; Rim, D. Dynamic Behavior of Indoor Ultrafine Particles (2.3−64 nm) Due to Burning Candles in a Residence. *Indoor Air* **2019**, *29* (6), 1018−1027.

(32) Jathar, S. H.; Sharma, N.; Bilsback, K. R.; Pierce, J. R.; Vanhanen, J.; Gordon, T. D.; Volckens, J. Emissions and Radiative Impacts of Sub-10 nm Particles from Biofuel and Fossil Fuel Cookstoves. *Aerosol Sci. Technol.* **2020**, *54* (10), 1231−1243.

(33) Rönkkö, T.; Kuuluvainen, H.; Karjalainen, P.; Keskinen, J.; Hillamo, R.; Niemi, J. V.; Pirjola, L.; Timonen, H. J.; Saarikoski, S.; Saukko, E.; Järvinen, A.; Silvennoinen, H.; Rostedt, A.; Olin, M.; Yli-Ojanperä, J.; Nousiainen, P.; Kousa, A.; Dal Maso, M. Traffic is a Major Source of Atmospheric Nanocluster Aerosol. *Proc. Natl. Acad. Sci. U. S. A.* **2017**, *114* (29), 7549−7554.

(34) Alanen, J.; Saukko, E.; Lehtoranta, K.; Murtonen, T.; Timonen, H.; Hillamo, R.; Karjalainen, P.; Kuuluvainen, H.; Harra, J.; Keskinen, J.; Rönkkö, T. The Formation and Physical Properties of the Particle Emissions from a Natural Gas Engine. *Fuel* **2015**, *162*, 155−161.

(35) Dada, L.; Stolzenburg, D.; Simon, M.; Fischer, L.; Heinritzi, M.; Wang, M.; Xiao, M.; Vogel, A. L.; Ahonen, L.; Amorim, A.; Baalbaki, R.; Baccarini, A.; Baltensperger, U.; Bianchi, F.; Daellenbach, K. R.; DeVivo, J.; Dias, A.; Dommen, J.; Duplissy, J.; Finkenzeller, H.; et al. Role of Sesquiterpenes in Biogenic New Particle Formation. *Sci. Adv.* **2023**, *9* (36), No. eadi5297.

(36) Cai, R.; Deng, C.; Stolzenburg, D.; Li, C.; Guo, J.; Kerminen, V.-M.; Jiang, J.; Kulmala, M.; Kangasluoma, J. Survival Probability of New Atmospheric Particles: Closure between Theory and Measurements from 1.4 to 100 nm. *Atmos. Chem. Phys.* **2022**, *22* (22), 14571−14587.

(37) Patel, S.; Rim, D.; Sankhyan, S.; Novoselac, A.; Vance, M. E. Aerosol Dynamics Modeling of Sub-500 nm Particles during the HOMEChem Study. *Environ. Sci.: Processes Impacts* **2021**, *23* (11), 1706−1717.

(38) Kerminen, V.-M.; Chen, X.; Vakkari, V.; Petäjä, T.; Kulmala, M.; Bianchi, F. Atmospheric New Particle Formation and Growth: Review of Field Observations. *Environ. Res. Lett.* **2018**, *13* (10), 103003.

(39) Kulmala, M.; Vehkamäki, H.; Petäjä, T.; Dal Maso, M.; Lauri, A.; Kerminen, V.-M.; Birmili, W.; McMurry, P. H. Formation and Growth Rates of Ultrafine Atmospheric Particles: A Review of Observations. *J. Aerosol Sci.* **2004**, *35* (2), 143−176.

(40) Amouei Torkmahalleh, M.; Turganova, K.; Zhigulina, Z.; Madiyarova, T.; Adotey, E. K.; Malekipirbazari, M.; Buonanno, G.; Stabile, L. Formation of Cluster Mode Particles (1−3 nm) in Preschools. *Sci. Total Environ.* **2022**, *818*, 151756.

(41) Poikkimäki, M.; Koljonen, V.; Leskinen, N.; Närhi, M.; Kangasniemi, O.; Kausiala, O.; Dal Maso, M. Nanocluster Aerosol Emissions of a 3D Printer. *Environ. Sci. Technol.* **2019**, *53* (23), 13618−13628.

(42) Kreyling, W. G.; Hirn, S.; Möller, W.; Schleh, C.; Wenk, A.; Celik, G.; Lipka, J.; Schäffler, M.; Haberl, N.; Johnston, B. D.; Sperling, R.; Schmid, G.; Simon, U.; Parak, W. J.; Semmler-Behnke, M. Air−Blood Barrier Translocation of Tracheally Instilled Gold Nanoparticles Inversely Depends on Particle Size. *ACS Nano* **2014**, *8* (1), 222−233.

(43) Oberdörster, G.; Sharp, Z.; Atudorei, V.; Elder, A.; Gelein, R.; Kreyling, W.; Cox, C. Translocation of Inhaled Ultrafine Particles to the Brain. *Inhal. Toxicol.* **2004**, *16* (6−7), 437−445.

(44) McWhinney, R. D.; Badali, K.; Liggio, J.; Li, S.-M.; Abbatt, J. P. D. Filterable Redox Cycling Activity: A Comparison between Diesel Exhaust Particles and Secondary Organic Aerosol Constituents. *Environ. Sci. Technol.* **2013**, *47* (7), 3362−3369.

(45) Khan, F.; Kwapiszewska, K.; Zhang, Y.; Chen, Y.; Lambe, A. T.; Kołodziejczyk, A.; Jalal, N.; Rudzinski, K.; Martínez-Romero, A.; Fry, R. C.; Surratt, J. D.; Szmigielski, R. Toxicological Responses of α-Pinene-Derived Secondary Organic Aerosol and its Molecular Tracers in Human Lung Cell Lines. *Chem. Res. Toxicol.* **2021**, *34* (3), 817−832.

(46) Wang, S.; Ye, J.; Soong, R.; Wu, B.; Yu, L.; Simpson, A. J.; Chan, A. W. H. Relationship between Chemical Composition and Oxidative Potential of Secondary Organic Aerosol from Polycyclic Aromatic Hydrocarbons. *Atmos. Chem. Phys.* **2018**, *18* (6), 3987−4003.

(47) Pye, H. O. T.; Ward-Caviness, C. K.; Murphy, B. N.; Appel, K. W.; Seltzer, K. M. Secondary Organic Aerosol Association with Cardiorespiratory Disease Mortality in the United States. *Nat. Commun.* **2021**, *12* (1), 7215.